


Quantum transport of strongly interacting fermions in one dimension far out of equilibrium

Jie Zou¹ and Xiaopeng Li^{1,2,*}

¹State Key Laboratory of Surface Physics, Institute of Nanoelectronics and Quantum Computing, and Department of Physics, Fudan University, Shanghai 200433, China

²Shanghai Qi Zhi Institute, AI Tower, Xuhui District, Shanghai 200232, China

 (Received 28 June 2022; revised 12 October 2022; accepted 19 October 2022; published 28 November 2022)

In the study of quantum transport, much has been known about dynamics near thermal equilibrium. However, quantum transport far away from equilibrium is much less well understood—the linear response approximation does not hold for physics far out of equilibrium in general. In this work, motivated by recent cold atom experiments on probing quantum many-body dynamics of a one-dimensional XXZ spin chain, where a transition from ballistic to diffusive dynamics has been established by increasing the interaction strengths, we study the strong interaction limit of the one-dimensional spinless fermion model, which is dual to the XXZ spin chain. We develop a highly efficient computation algorithm for simulating the nonequilibrium dynamics of this system exactly, and examine the nonequilibrium dynamics starting from a density modulation quantum state. We find ballistic transport in this strongly correlated setting and show that a plane-wave description emerges at long-time evolution. We also observe a sharp distinction between transport velocities in short and long times as induced by interaction effects and provide a quantitative interpretation for the long-time transport velocity. We expect our results to shed light on the understanding of the dynamics of the XXZ spin chain in the strong interaction regime.

DOI: [10.1103/PhysRevA.106.053321](https://doi.org/10.1103/PhysRevA.106.053321)

I. INTRODUCTION

Transport in low-dimensional quantum systems [1] has been attracting continuous research interest from both theoretical and experimental perspectives, due to both the existence of solvable models [2] and intrinsic strong correlation effects [1,3]. Although wave functions are exactly solvable via Bethe ansatz (BA) [4] in certain one-dimensional (1D) models, it is challenging to compute dynamical observables such as transport properties with analytic methods. Phenomenons unveiled by recent studies still demand advanced numerical techniques to explain [5–7].

The spin-1/2 XXZ chain in one dimension is a representative spin model, with the Hamiltonian

$$H = J \sum_{i=1}^L (S_i^x S_{i+1}^x + S_i^y S_{i+1}^y + \Delta S_i^z S_{i+1}^z), \quad (1)$$

where L is the system size, J denotes the hopping strength, and Δ labels the spin anisotropy. Despite its simplicity, this model exhibits several interesting transport properties worth theoretical investigation. New concepts in nonequilibrium dynamics in closed quantum systems [8,9], including the generalized Gibbs ensemble [10], can also be studied in this model with a quantum quench setup [11]. Another reason is from the perspective of phenomenological transport laws. The existence of anomalous transport at finite temperatures, which does not obey Fourier's law [12], has been proved via linear-response theory [13] in this model.

Previous studies on one-dimensional quantum spin transport in the linear response regime have provided important insights about the correlated quantum dynamics. It has been proved that finite-temperature transport is ballistic for $|\Delta| < 1$ (gapless phase) at zero magnetization ($m_z = \sum_i \langle s_i^z \rangle / L = 0$) [14] or for generic Δ at finite magnetization [13,15]. For nonzero magnetization, Mazur inequality [16] gives a finite lower bound [13,15] for the spin Drude weight $D_W^{(s)}$ [17], which indicates a ballistic transport. The theoretical study at high temperature [13] finds

$$D_W^{(s)} \geq \frac{J^2 \Delta^2 m_z^2}{4T} \frac{1 - m_z^2}{1 + \Delta^2 (2 + 2m_z^2)} > 0. \quad (2)$$

At the same time, for $m_z = 0$, besides the ballistic transport in the gapless phase ($|\Delta| < 1$), recent studies also suggest [18–20] a diffusive transport in the gapped phase ($|\Delta| > 1$) and predict [21] a superdiffusive transport in the Heisenberg limit ($|\Delta| \rightarrow 1$).

In contrast to the linear-response regime, dynamics far out of equilibrium is less well studied. The results obtained via linear-response theory may not hold at far out of equilibrium. Numerical methods, such as the commonly used density matrix renormalization group (DMRG) algorithm [22], tend to be limited in simulating long-time quantum dynamics due to the rapid entanglement growth. Finding solvable models or efficient algorithms is thus important for investigating far-out-of-equilibrium dynamics.

The study of far-out-of-equilibrium quantum transport becomes more desirable with recent developments in cold atom experiments. Experiments based on such clean and

*xiaopeng_li@fudan.edu.cn

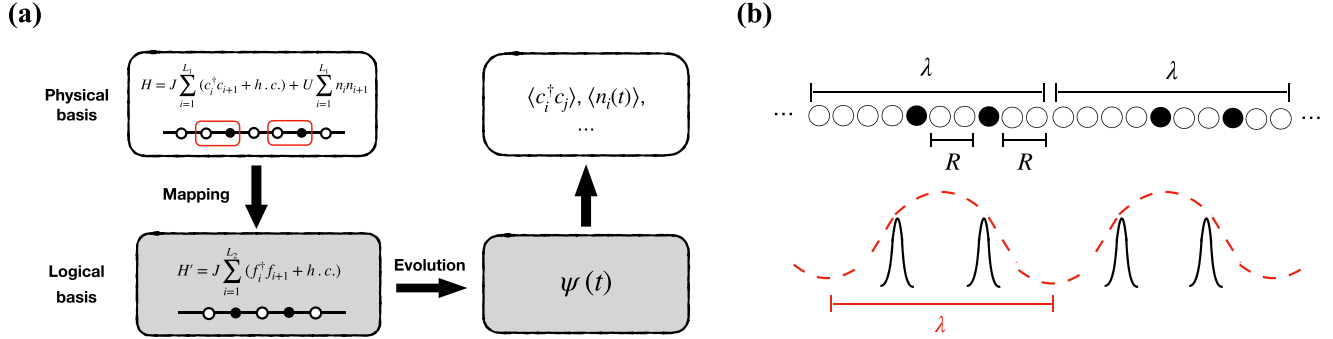


FIG. 1. (a) Workflow of the algorithm solving the strongly interacting model. The dynamics can be efficiently computed in logical basis by mapping the interacting model to a free one. The physical observables are computed by mapping back to interacting basis [23,24], for which the key is to sample the Slater determinant wave function efficiently. Here we implement the recently developed fast fermion sampling algorithm [25], in order to simulate large system sizes. (b) Illustration of the density modulation state. The black (white) circles represent occupied (empty) sites. In this state, the particles are distributed in a periodic way with a period λ and are separated by a distance R . Without loss of generality, we put the remaining $\lambda - n(R + 1)$ empty sites on the left of a period as a padding, with n the particle number in each period.

controllable closed quantum systems [26] are naturally suitable to study the nonequilibrium dynamics, stimulating much recent research effort in this direction [5,7,27]. Notably, a recent experiment [7] demonstrates a subdiffusive transport for the spin helix state, instead of the diffusive behavior predicted by linear-response theory analysis [18,20], in a gapped phase at zero magnetization for the anisotropic Heisenberg model. The experiment on the isotropic case also shows a violation of the linear-response approximation when considering high-energy-density spin spiral states [5]. Modeling and understanding the far-out-of-equilibrium quantum transport of the one-dimensional spin chain demands further theoretical investigation.

In this work, we focus on a one-dimensional spinless fermion model, which is equivalent to the spin-1/2 XXZ model. We take a strong interaction limit, in which physical observables can be efficiently calculated with our fast fermion sampling algorithm [23–25]. Due to the infinitely large repulsion, we can only deal with cases away from half-filling (zero magnetization). In the strong interaction limit, it has been shown by linear response theory that the spin current operator has full overlap with the energy current away from half filling, which implies ballistic transport [13]. In this work, we focus on the far-out-of-equilibrium quantum dynamics. We choose the density modulation state (DMS), a highly excited state, beyond the description of linear response theory. The setup of the DMS state is demonstrated in Fig. 1(b). Our results show that the far-out-of-equilibrium quantum evolution develops ballistic transport even for the infinite-temperature ensemble. Furthermore, we provide a plane-wave picture in describing the long-time dynamics of this highly excited state in the strongly interacting model. At last, we observe different transport velocities in short and long times caused by interaction effects. The transport velocity in the long-time limit is described by our plane-wave picture.

II. MODEL AND METHODS

A. One-dimensional strongly interacting fermion model

We consider a strongly interacting fermionic model on a one-dimensional lattice, with particle number N and the

site index $i \in [1, L]$. The quantum many-body dynamics is described by a Hamiltonian,

$$H = -J \sum_{i=1}^{L_1} (c_i^\dagger c_{i+1} + \text{H.c.}) + U \sum_{i=1}^{L_1} \sum_{k=1}^R n_i n_{i+k}, \quad (3)$$

with i the lattice site index, c_i the fermionic annihilation operator, and $n_i = c_i^\dagger c_i$ the occupation number. Here we take the strongly interacting limit $U \rightarrow +\infty$ and J is the tunneling strength. The interaction range R and the filling $\rho = N/L$ are both tunable parameters in our model. In this work, we choose an open boundary condition and set the lattice constant and tunneling to be the length and energy units, respectively. In fact, this fermionic model is equivalent to a spin-1/2 XXZ model through a Jordan-Wigner transformation [4]. Notably, all the dynamics are suppressed in this strong interaction limit when the system is at half-filling, or equivalently at zero magnetization in the corresponding spin model. Therefore, in this work, we carry out our theoretical study away from half-filling.

B. An efficient algorithm

To overcome the exponential complexity of the interacting many-body system, here we adapt an efficient sampling algorithm [24,25] to compute the time evolution, with an $O(M_s L N^2)$ complexity and an error δ proportional to the inverse square root of M_s , the number of random samples. The illustration of this method is shown in Fig. 1(a).

Since we take the infinite interaction limit, those states with two particles in a neighborhood of size R are prohibited. Taking this constraint into account, we can map our model to an exactly solvable free fermion case [23,24]. This is realized by considering one occupied site and R empty sites on its left as a composite fermion. For theoretical convenience, we append R empty sites at the left boundary, because otherwise we cannot construct the composite fermion above when there is a fermion in the leftmost R sites—only when we append these empty sites could we make a one-to-one mapping [23,24]. Through this mapping, the particle number remains the same as the original model and the system size is reduced to $L_2 =$

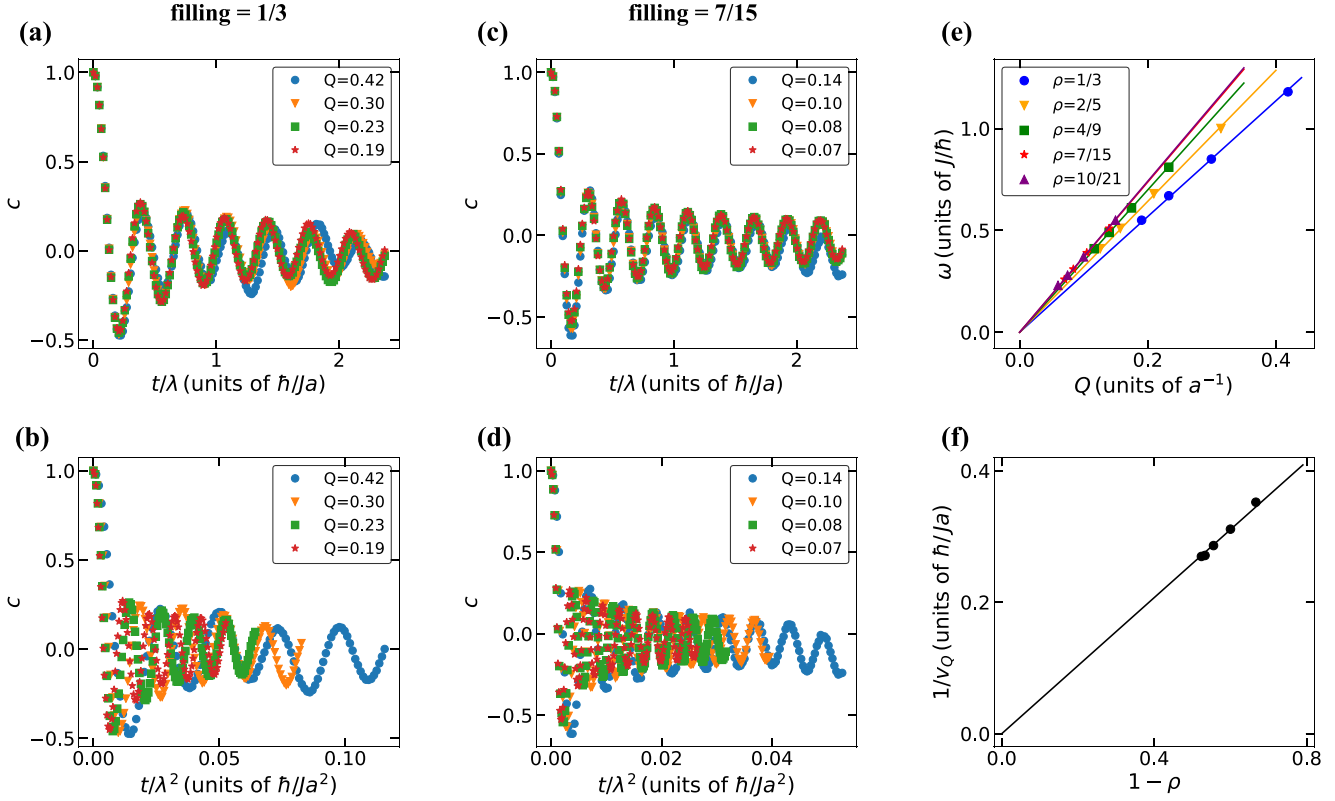


FIG. 2. Relaxation of the density modulation state. The interaction range here is fixed to $R = 1$. (a, b) The normalized contrast, $c(t)$ in Eq. (5), with different wave vectors Q , at filling $\rho = 1/3$. The evolution time t is rescaled by the wavelength λ and its square λ^2 in (a) and (b), respectively. (c, d) Time evolution of the normalized contrast at a different filling, $\rho = 7/15$. (e) Long-time oscillation frequency ω of the contrast as a function of the wave vector Q . The numerical data points are well fitted by a linear function $\omega = v_Q Q$, with v_Q the dispersion velocity. The slopes v_Q are 2.84, 3.21, 3.49, 3.69, and 3.71 for filling factors $\rho = 1/3, 2/5, 4/9, 7/15$, and $10/21$. (f) Dependence of v_Q on the filling. A nontrivial linear relation between the inverse of dispersion velocity and the filling factor is uncovered. We find $1/v_Q \approx 0.52 \times (1 - \rho)$ by an empirical fitting.

$L_1 - R(N - 1)$. Hereafter, we refer to the model before (after) the mapping as the one in physical (logical) basis. Here we point out that this is a highly nonlocal mapping which leads to some nontrivial properties, such as “ball-like” behavior in OTOC spreading [24].

Furthermore, an advanced fermion sampling method benefits us with less time cost when solving the free fermion problem. Contrary to the commonly used DMRG [22] method, which only allows an investigation on systems up to hundreds of sites in short and intermediate times, our algorithm can solve the dynamics exactly regardless of the evolution time, for a large system with up to thousands of sites.

C. Density modulation state

Taking the interacting fermion model, we consider the time evolution of a density modulation state, which has a similar periodic structure as in spin helix states investigated in recent experiments [5,7] through Jordan Wigner transformation. It is a highly excited state since the expectation value of its energy is equal to zero, corresponding to the infinite temperature ensemble average (see Appendix). The preparation of this state is shown in Fig. 1(b). Fermions are arranged in a periodic structure with λ as the wavelength, and thus the

particle number in a period is determined for a given filling ρ . Within a period, these particles are aligned in a most compact pattern, that is, the distance of two adjacent particles is set to be the interaction range R . Then we still have $\lambda - n(R + 1)$ empty sites remaining in each period, which we put on the left of a period as a padding, with n as the particle number in each period. At last, a suitable system size is also necessary to minimize the finite size effect and the computation cost, which we set as $L = 4\lambda$ in this work.

III. RELAXATION

The relaxation dynamics is characterized by examination of the density modulation amplitude. Due to the periodicity of density modulation states, the contrast of density modulation is defined through a Fourier transform,

$$C(t) = \frac{2}{L} \sum_{i=1}^L \langle n_i(t) \rangle \cos(Qi), \tag{4}$$

where $Q = 2\pi/\lambda$ is the wave vector. For comparison, we focus on the normalized contrast

$$c(t) = C(t)/C(0). \tag{5}$$

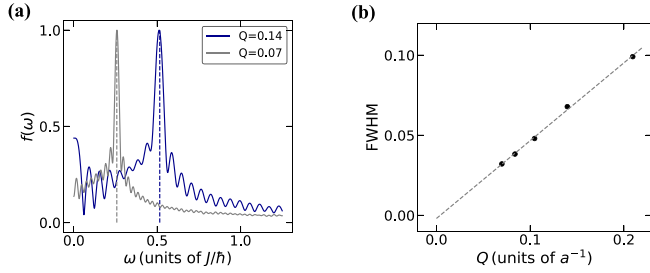


FIG. 3. A frequency analysis on the oscillations of normalized contrast. (a) The frequency spectrum of the oscillations. The dashed line denotes the position of the extracted frequency, $\omega = v_Q Q$, from the analysis shown in Fig. 2, with v_Q the dispersion velocity. (b) Full width at half maxima (FWHM) of the peaks. The numerical results are well fitted by a linear function. The computation above is implemented when $\rho = 7/15$ and $R = 1$.

This physical observable is also commonly used to characterize a spin helix state in recent experiments [7].

In the linear response regime, whether a system is half-filled plays a key role in its transport property [13,14]. One of the main purposes of our work is to investigate the strong interaction effects on the quantum transport. We set the filling $\rho = \frac{m}{2m+1}$ ($m = 1, 2, \dots$) so that we can gradually probe the half-filling limit. The results are shown in Fig. 2.

We observe a data collapse in the density wave contrast [$C(t)$ in Eq. (4)], with the evolution time (t) rescaled by the wavelength λ . This data collapse holds even for a filling factor quite close to $1/2$ ($\rho = 7/15$). This data-collapse behavior is absent if the time t is rescaled by the square of the wavelength λ^2 instead. These numerical results imply universal ballistic transport in this model, despite the strong interaction induced nonlinearity.

We further study the oscillation of the normalized contrast $c(t)$ via an analysis on the frequency spectrum $f(\omega)$, which is defined by a Fourier transformation of $c(t)$ to the frequency domain. For convenience, we normalize the frequency spectrum and compare the results with different wave vectors Q in the initial DMS. In Fig. 3(a), the frequency spectrum shows a sharp peak at $\omega = v_Q Q$, with v_Q being the corresponding dispersion velocity. The full width at half maxima (FWHM) of the peaks for different Q is shown in Fig. 3(b). We find a linear relation between FWHM and wave vector Q , which is consistent with the data collapse as shown in Fig. 2. The FWHM of the peak in the frequency spectrum also implies that the decay of the normalized contrast is attributed to dephasing effects.

Since the quantum transport in this model is ballistic, we make an analog with plane wave propagating in free space with a certain velocity. Surprisingly, the ballistic transport that emerges from the far-out-of-equilibrium DMS state in our strongly interacting model is captured by a physical picture of propagating plane wave in free space. For a massless plane wave mode spreading in free space with wave vector k and energy $E = \hbar\omega$, the dispersion relation is $\omega = vk$, where v is a dispersion velocity that determines the ballistic transport velocity of the plane wave in free space. In our model, we find that the linear dispersion emerges $\omega_Q = v_Q Q$ in the long-time oscillation dynamics of the DMS state for a broad range

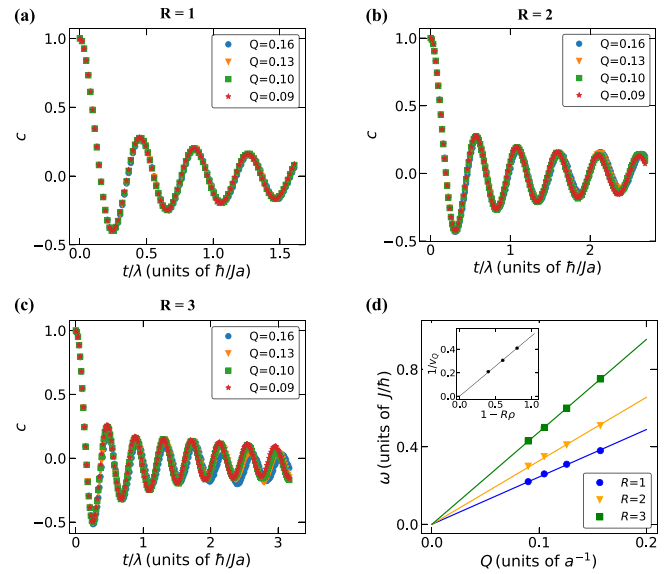


FIG. 4. Dependence of density modulation relaxation dynamics on the interaction range. (a–c) normalized contrast $c(t)$ [Eq. (5)] with interaction ranges $R = 1, 2$, and 3 . We investigate the relaxation dynamics for a broad range of wave vector Q from 0.09 to 0.16 . The evolution time t is rescaled by the wavelength λ . (d) Long-time oscillation frequency of the contrast. The numerical data points are all captured by the linear relation $\omega = v_Q Q$. The dispersion velocities v_Q are $2.44, 3.28$, and 4.77 for the interaction range $R = 1, 2$, and 3 , respectively. Its inset shows the linear relation between the inverse of the dispersion velocity v_Q and the interaction range R . The filling ρ is fixed to $1/5$ here.

of wave vector Q (Fig. 2). Besides, the dispersion velocity extracted from the long-time oscillation quantitatively agrees with the spreading velocity [see Fig. 5(c)]. These numerical results imply that the quantum dynamics of the strongly interacting fermions in one dimension starting from the far-out-of-equilibrium DMS state is well captured by a physical picture of propagating dynamics of a massless plane wave mode. The strong interaction effects on the dynamics are reflected by the nontrivial dependence of the dispersion velocity v_Q on the filling ρ [Fig. 2(f)], to be further elaborated on in the later analysis of velocity renormalization.

To confirm the generality of our finding, we further investigate the relaxation dynamics at different interaction ranges R . The results are shown in Fig. 4. We observe that for $R = 1, 2$, and 3 , the relaxation dynamics starting from DMS states with different wavelengths λ all collapse on a curve when time t is rescaled by λ . This confirms the ballistic transport for the different choices of interaction ranges. We find that the dispersion velocity extracted from late-time oscillation dynamics becomes larger as we increase the interaction range R [Fig. 4(d)]. This can be attributed to the fact that the longer interaction range in our model tends to accelerate the dynamical transport.

IV. VELOCITY RENORMALIZATION

Velocity is a characteristic property of ballistic transport, as well as an observable which can be measured directly

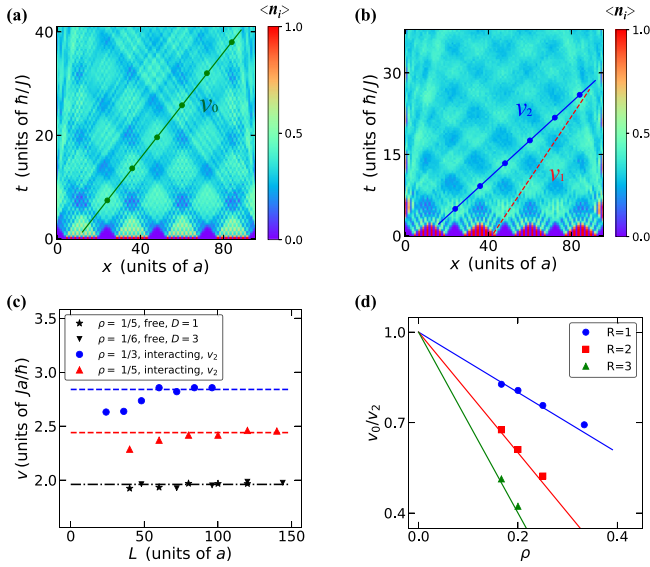


FIG. 5. Sound velocity renormalization. (a, b) Time evolution of the density profile $\langle n_i(t) \rangle$ for free and interacting fermions, respectively. The sound velocities are determined according to the propagation of the wave front as marked by the green line in (a) and the blue and red lines in (b). The free fermion dynamics is characterized by one velocity scale, v_0 , whereas the two different velocities, v_1 and v_2 , appear in the early and late stages of the interacting dynamics. In (b), we choose a system size $L = 96$, particle number $N = 32$, and wavelength $\lambda = 24$. The initial state is a density modulation state as shown in Fig. 1. We use the same setup for noninteracting fermions in (a) for a fair comparison. (c) Convergence of the propagating velocities with increasing the system size. The velocities for the noninteracting model (black triangles and stars), with different fillings ρ and particle separations within a period D , converge to $v = 1.96$ (black dotted line). The velocity v_2 for interacting fermions (blue dots and red triangles) converges to the dispersion velocity v_Q (dashed lines), as extracted from long-time oscillation of the dynamics. In (a)–(c), we choose $R = 1$. (d) The ratio between v_0 and v_2 as a function of the filling ρ . The numerical results are well fitted by a linear function.

in experiments. In our numerical simulation here, we determine the sound velocity by extracting the slope of the stripe pattern in the density profile $\langle n_i(t) \rangle$. A typical time evolution of $\langle n_i(t) \rangle$ is shown in Fig. 5(a) [5(b)] considering the density modulation state in the free (strongly interacting) model. The free fermion velocity v_0 and the short-time (long-time) velocity v_1 (v_2) in the interacting case is also determined by fitting the stripe pattern in Fig. 5(a) [5(b)]. The strongly interacting model shows different behaviors at early and late time evolution. This two-stage dynamical feature as originated from strong interaction effects makes the system distinctive from noninteracting fermions. Moreover, even at late time where the ballistic transport of the strongly interacting model looks similar to the noninteracting case, the propagating velocity is actually strongly renormalized by the interaction.

To gain more insight into the renormalization process, we quantitatively study the velocities mentioned above. As the system size grows, the free fermion velocity v_0 and the long-

time velocity v_2 in the interacting case converge, which is demonstrated in Fig. 5(c). For comparison, we also choose DMS states as initial states in the noninteracting case. Again, the particles are aligned in a periodic way [see Fig. 1(b)], with D the distance between particles within a period, in analog with R in the interacting case. It is shown that the converged value of v_0 is independent of D and filling ρ , as expected for free fermions. Hereafter, the velocities v_0 and v_2 are defined according to their thermodynamic limits. We observe that the velocity v_2 matches the dispersion velocity v_Q extracted from the long-time oscillations. The linear fit in Fig. 5(d) suggests the relation $v_0/v_2 = 1 - R\rho$. This is verified in our numerical calculation for a broad range of R and ρ .

The renormalization of the velocity in the interacting dynamics as compared to the noninteracting case can be understood from the mapping between the logical and physical basis. In this mapping, a length scale l in the physical basis (interacting) shrinks to $l - lR\rho$ in the logical basis (noninteracting) on average. Such shrinking has been used in the previous study on the ground state of the 1D strongly interacting fermions for the Luttinger parameter [23]. In our study of the dynamics, since the long-time behavior of the strongly interacting model is captured by the plane-wave picture, it is reasonable to expect that the velocity renormalizes according to the length scale, which then implies

$$\frac{v_0}{v_2} \simeq 1 - R\rho. \tag{6}$$

This is exactly the same as what we observed in our numerical simulations.

V. CONCLUSION

In this work, we study the quantum transport properties of strongly interacting spinless fermions in one dimension. This model is simulated efficiently using a fast fermion sampling algorithm at the strong interaction limit. Despite the strong interaction, we observe robust ballistic transport for different fillings and interaction ranges. The ballistic transport has two stages in dynamics with different transport velocities. We propose a plane-wave description for the ballistic transport of the strongly interacting fermions, which captures the long-time dynamics. The predominant effect of the strong interaction on the transport is to introduce velocity renormalization. Our results indicate that the subdiffusive transport observed for the weakly interacting spin chain in the experiment [7] would have a crossover to ballistic behavior when approaching the strongly interacting regime. This is worth further experimental investigation.

ACKNOWLEDGMENTS

We acknowledge support by the National Program on Key Basic Research Project of China (Grant No. 2021YFA1400900), the National Natural Science Foundation of China (Grant No. 11934002), Shanghai Municipal Science and Technology Major Project (Grant No. 2019SHZDZX01), and the Shanghai Science Foundation (Grants No. 21QA1400500 and No. 19ZR1471500).

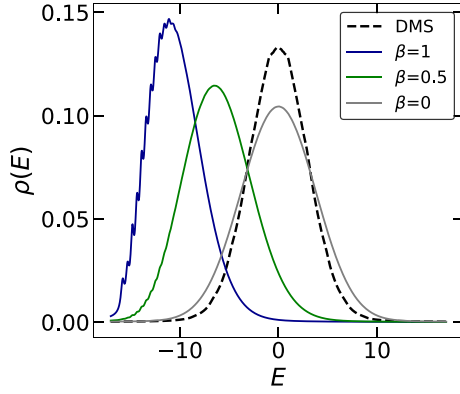


FIG. 6. The energy distribution of DMS and canonical ensembles at different temperatures. The energy distribution of DMS is computed on a 36-site chain with 12 particles aligned according to the rules of DMS with wavelength $\lambda = 9$. The same setup (system size and particle number) is used to calculate the energy distribution of canonical ensembles at different temperatures. The mean energy of DMS and the infinite temperature canonical ensemble are both equal to zero. Here the delta function is approximated via a Lorentzian with width $\epsilon = 0.2$.

APPENDIX: CORRESPONDENCE BETWEEN DENSITY MODULATION STATE AND INFINITE TEMPERATURE ENSEMBLE RESULTS

In the main text, we informally give a correspondence between DMS and infinite temperature ensemble results, con-

sidering that they have the same average energy. In this part, we will validate this correspondence more seriously from the perspective of energy distribution.

We compare the energy distribution of DMS with that in canonical ensembles with different temperatures, as shown in Fig. 6. The energy distribution of DMS is given by

$$\rho_{\text{DMS}}(E) = \sum_i \delta(E - E_i) |\psi_i|^2, \quad (\text{A1})$$

with i indexing the many-body eigenstates, E_i the eigenenergy, and $|\psi_i|^2$ the overlap between DMS and the corresponding eigenstate. The energy distribution of a canonical ensemble with an inverse temperature β is given by

$$\rho_\beta(E) = \sum_i \delta(E - E_i) e^{-\beta E_i} / Z, \quad (\text{A2})$$

with the partition function $Z = \sum_i e^{-\beta E_i}$. In a finite-size calculation, we approximate the delta function via a Lorentzian,

$$\delta(E) = \frac{1}{\pi} \lim_{\epsilon \rightarrow 0} \frac{\epsilon}{\epsilon^2 + E^2}, \quad (\text{A3})$$

where we take a small but finite width ϵ in practice.

In Fig. 6, we observe that the energy distribution of DMS is much closer to that of the infinite temperature ensemble ($\beta = 0$), in terms of their mean energy and energy fluctuation. We thus take the results derived from the DMS state as an analogy in the high-temperature limit.

-
- [1] B. Bertini, F. Heidrich-Meisner, C. Karrasch, T. Prosen, R. Steinigeweg, and M. Žnidarič, Finite-temperature transport in one-dimensional quantum lattice models, *Rev. Mod. Phys.* **93**, 025003 (2021).
 - [2] M. Takahashi, *Thermodynamics of One-Dimensional Solvable Models* (Cambridge University Press, Cambridge, 2005).
 - [3] V. B. Bulchandani, S. Gopalakrishnan, and E. Ilievski, Superdiffusion in spin chains, *J. Stat. Mech.: Theory Exp.* (2021) 084001.
 - [4] T. Giamarchi, *Quantum Physics in One Dimension*, (Clarendon Press, Oxford, 2003), Vol. 121.
 - [5] S. Hild, T. Fukuhara, P. Schauß, J. Zeiher, M. Knap, E. Demler, I. Bloch, and C. Gross, Far-From-Equilibrium Spin Transport in Heisenberg Quantum Magnets, *Phys. Rev. Lett.* **113**, 147205 (2014).
 - [6] J. P. Ronzheimer, M. Schreiber, S. Braun, S. S. Hodgman, S. Langer, I. P. McCulloch, F. Heidrich-Meisner, I. Bloch, and U. Schneider, Expansion Dynamics of Interacting Bosons in Homogeneous Lattices in One and Two Dimensions, *Phys. Rev. Lett.* **110**, 205301 (2013).
 - [7] P. N. Jepsen, J. Amato-Grill, I. Dimitrova, W. W. Ho, E. Demler, and W. Ketterle, Spin transport in a tunable Heisenberg model realized with ultracold atoms, *Nature (London)* **588**, 403 (2020).
 - [8] J. Eisert, M. Friesdorf, and C. Gogolin, Quantum many-body systems out of equilibrium, *Nat. Phys.* **11**, 124 (2015).
 - [9] L. D'Alessio, Y. Kafri, A. Polkovnikov, and M. Rigol, From quantum chaos and eigenstate thermalization to statistical mechanics and thermodynamics, *Adv. Phys.* **65**, 239 (2016).
 - [10] M. Rigol, V. Dunjko, V. Yurovsky, and M. Olshanii, Relaxation in a Completely Integrable Many-Body Quantum System: An *Ab Initio* Study of the Dynamics of the Highly Excited States of 1D Lattice Hard-Core Bosons, *Phys. Rev. Lett.* **98**, 050405 (2007).
 - [11] M. Rigol, V. Dunjko, and M. Olshanii, Thermalization and its mechanism for generic isolated quantum systems, *Nature (London)* **452**, 854 (2008).
 - [12] T. N. Narasimhan, Fourier's heat conduction equation: History, influence, and connections, *Rev. Geophys.* **37**, 151 (1999).
 - [13] X. Zotos, F. Naef, and P. Prelovsek, Transport and conservation laws, *Phys. Rev. B* **55**, 11029 (1997).
 - [14] T. Prosen, Exact Nonequilibrium Steady State of a Strongly Driven Open *xxz* Chain, *Phys. Rev. Lett.* **107**, 137201 (2011).
 - [15] H. Castella, X. Zotos, and P. Prelovšek, Integrability and Ideal Conductance at Finite Temperatures, *Phys. Rev. Lett.* **74**, 972 (1995).
 - [16] P. Mazur, Non-ergodicity of phase functions in certain systems, *Physica* **43**, 533 (1969).

- [17] D. J. Scalapino, S. R. White, and S. Zhang, Insulator, metal, or superconductor: The criteria, *Phys. Rev. B* **47**, 7995 (1993).
- [18] E. Ilievski and J. De Nardis, Microscopic Origin of Ideal Conductivity in Integrable Quantum Models, *Phys. Rev. Lett.* **119**, 020602 (2017).
- [19] C. Karrasch, J. E. Moore, and F. Heidrich-Meisner, Real-time and real-space spin and energy dynamics in one-dimensional spin- $\frac{1}{2}$ systems induced by local quantum quenches at finite temperatures, *Phys. Rev. B* **89**, 075139 (2014).
- [20] N. M. R. Peres, P. D. Sacramento, D. K. Campbell, and J. M. P. Carmelo, Curvature of levels and charge stiffness of one-dimensional spinless fermions, *Phys. Rev. B* **59**, 7382 (1999).
- [21] J. De Nardis, M. Medenjak, C. Karrasch, and E. Ilievski, Universality Classes of Spin Transport in One-Dimensional Isotropic Magnets: The Onset of Logarithmic Anomalies, *Phys. Rev. Lett.* **124**, 210605 (2020).
- [22] U. Schollwöck, The density-matrix renormalization group in the age of matrix product states, *Ann. Phys.* **326**, 96 (2011).
- [23] G. Gómez-Santos, Generalized Hard-Core Fermions in One Dimension: An Exactly Solvable Luttinger Liquid, *Phys. Rev. Lett.* **70**, 3780 (1993).
- [24] X. Li, G. Zhu, M. Han, and X. Wang, Quantum information scrambling through a high-complexity operator mapping, *Phys. Rev. A* **100**, 032309 (2019).
- [25] H. Sun, J. Zou, and X. Li, Fermion sampling made more efficient (2021), [arXiv:2109.07358](https://arxiv.org/abs/2109.07358).
- [26] I. Bloch, J. Dalibard, and W. Zwerger, Many-body physics with ultracold gases, *Rev. Mod. Phys.* **80**, 885 (2008).
- [27] T. Fukuhara, P. Schauß, M. Endres, S. Hild, M. Cheneau, I. Bloch, and C. Gross, Microscopic observation of magnon bound states and their dynamics, *Nature (London)* **502**, 76 (2013).